Fully Active Neutrino Target Assembly

M. Atiya, R. Fine, E. Hartouni, S. Kim, W. Lee*,
C. Ma†, R. Seto, P. Sokolsky, R. Zhu‡
Columbia University, New York, N.Y. 10027

M. Lamm, T. O'Halloran, Jr., J. Wiss
University of Illinois, Urbana, Ill. 61801

* Spokesperson

†, ‡ On Leave from the Institute
of High Energy Physics, P.R.C.

April 1980

Introduction

We propose the construction of a 100% active low density ν target (as opposed to a CHARM or E-594 type of calorimeter). In addition to the usual physics goals of most neutrino counter experiments, we concentrate on the ability to measure the angle and energy of hadrons and electrons well. This will allow us to study very small $P_\perp$ physics ($\nu e \rightarrow \nu e$) and search for $P_\perp$ imbalance in large $P_\perp$ final states (missing final state ν's). An example of the latter is τ production by ν_τ's and new flavor production.

We propose to calibrate our detector in the dichromatic beam to understand the energy and angular resolution of our ν target. This is why we originally proposed to place our detector in this neutrino beam. In the triplet beam our primary goal is to study multimuon final states with missing neutrino(s). This will include the study of the weak interaction of the bottom quark. In the beam dump our main goal is to study the interaction of ν_τ.

We have concentrated on designing a detector optimized to handle the high muon backgrounds expected in beam dump experiments and have provided for rapid online data reduction. In particular, the muon spectrometer we propose is designed à la Exp. 87A and is capable of rapid and efficient multitrack reconstruction. In the following, we will concentrate on ν_τ and new flavor production topics. Additional detectors are required to study $\nu e \rightarrow \nu e$ scattering. This is being studied by G. Barbiellini and his collaborators and an addendum by them will be submitted at a later time.

History

In early 1978, a series of beam dump experiments were performed by the CDHS, BEBC and GGM detector groups at CERN. The bubble chamber groups observed a ratio of neutrino induced electron events to neutrino induced muon events too large to be accounted for by ordinary sources. The CDHS group observed an anomalously large ratio of muonless events to ordinary charged current events.

In 1979, a second series of beam dump experiments was performed at 0 mrad by the CDHS, CHARM and BEBC groups. The experimenters varied the target density and improved beam monitoring to eliminate upstream scraping as a source of the anomaly observed in 1978. The conclusion from this series of experiments is clear: there exists a prompt source of neutrinos in proton-proton collisions which produces approximately equal numbers of electron and muon neutrinos. Such a source is presumably the production and decay of charmed particles.

Tevatron Beam Dump

There are several reasons why a beam dump experiment at the Tevatron will represent a significant improvement over experiments performed at 400 GeV.

First, in a wide variety of models, the $D\bar{D}$ cross section is expected to rise with incident proton energy faster in the region of 400-1000 GeV than ordinary π and k production. In particular, in the model of Bourquin-Gaillard, the increase is expected to be a factor of 2.1 (Fig. 1).

Second, a detector covering the forward direction will subtend a substantially larger fraction of the total prompt neutrino flux at 1000 GeV, since the production angles fold forward by $\gamma_{c.m.}$. Compared to 400 GeV, the flux through a fixed solid angle detector will increase by a factor of $\sim \gamma_{c.m.}^{2}$, or $\sim$ 2.5.

Third, the energy of the prompt neutrinos is higher for 1000 GeV than for 400 GeV protons. This implies a higher event rate in the detector by a factor of $\sim$ 2.5.

Fourth, as the energy of the ordinary π's and K's increases, the fraction of those which decay decreases as 1/E. Coupled with the relative increase in cross section for prompt sources, this implies an increase in signal/noise of $\sim$ 5. Prompt sources will dominate the ν flux from a Tevatron beam dump even at 0 mrad.

Finally, by increasing the incident proton energy, there is always the possibility of encountering something new, which may not be accessible at lower energies.

Beam Dump and Muon Filter

We propose that the neutrino area be modified to include a proton beam capable of transporting the full machine intensity and deliver it to a Cu total absorption target at 0 mrad. It is desirable that the proton beam angle be adjustable from 0 to 20 mrad for studies of the $P_{\perp}$ dependence of the prompt signal. We further propose that the upstream end of our detector be situated $\sim$ 400 ft downstream of the target. This corresponds to an angular acceptance of 7.5 mrad for the fiducial volume we have chosen.

The target will be followed by a magnetized iron muon filter. A detailed design for such a filter is prepared as a Fermilab TM . Because of the high speed of our detector, we estimate that we can survive with muon fluxes of $\leq 10^4$ μ/ pulse (1.5 ms pulse).

We believe that rapid turnaround in reconstruction of muon direction in the muon spectrometer will be essential in determining residual sources of muons and reduction of muon background in the early stages of this experiment, both for us and the other experiments in the beam.

Detector

Figure 2 shows a schematic of the detector. It consists of three parts: a target, composed of 200 tons of acrylic scintillator, a 200 ton hadron energy catcher composed of iron and scintillator, and a muon spectrometer. The 200 ton acrylic scintillator serves as a target for ν interactions and as a calorimeter and energy flow vector measuring device. The hadron energy catcher serves to contain and measure hadronic energy which leaks from the target. It also shields the muon spectrometer from hadronic shower spray.

We now consider each part in detail.

The Target

The target consists of eighty 12 ft x 12 ft x 6 in. acrylic scintillator planes (see Fig. 3). Each plane is composed of eighteen (8 in. x 6 in. x 12 ft) scintillator tubes, with each tube viewed from both ends by 2 in.

phototubes through lucite light pipes. Each plane represents 0.5 radiation length of material and adjacent planes are rotated by 90^{o} so that an x and y measurement of the shower profile is performed every radiation length. The overall length of the target is 40 ft. A total of 2,880 phototubes are required to view it.

The acrylic plastic is doped with 0.01% POPOP, 1% PPO and 5% naphthalene by weight and has a measured light yield of 25 photoelectrons/minimum ionizing particle at the center of the tube. The attenuation length is $\sim$ 2 m. Each scintillator tube is encased in a thin aluminum skin and is self-supporting and separately movable. Figure 4 shows details of the phototube assembly. Although no additional absorber is presently envisaged, the target support is designed so that additional absorber and/or drift chambers may be inserted between the planes at a later time.

The Hadron Catcher

The hadron catcher is composed of fifteen 14 ft x 14 ft x 4 in. Fe plates interspersed with 14 ft x 14 ft x 4 in. acrylic scintillator sheets. The acrylic scintillator is not segmented and the total light pulse from each sheet is read out by waveshifter bars to four phototubes located at the corners of the sheet. We have measured the light yield for such a configuration to be $\sim$ 20 photoelectrons/minimum ionizing particle. The total length of Fe is 5 ft and the total number of phototubes is 60.

Muon Spectrometer

The muon spectrometer is designed very much like the E-87A spectrometer. It is composed of three units of drift chambers in front of a torroidal magnet and followed by two units in the back. Each unit consists of four planes, each one rotated by 45^{o} with respect to the other. Figure 5 shows details of the plane construction. The torroid has a radius of 7 ft and has the bending power of 2 GeV/c. The main feature of the muon spectrometer compared to others used in neutrino experiments is rapid and efficient reconstruction of muons. We believe that this feature is needed for the beam dump part of the experiment. The spatial resolution of the drift chambers is assumed to be $\pm$ 0.5 mm. This gives

$$\frac{\Delta p}{p^2} \text{ (measurement error only)} = 1.4 \times 10^{-4}$$

and

$$\frac{\Delta p}{p} \text{ (multiple scattering)} = 10^{-1} \quad .$$

The vertex of the event can be located to better than 1 cm by tracing the muon track back to the beginning of the hadron shower.

Electronics

HV Distribution System

Each photomultiplier will have a dedicated HV supply, packaged 8/card in a standard crate system. The output voltage is programmable from a digital bus in steps of about 1 V over the photomultiplier operating range. This is done by comparing the output of a precision voltage divider

with a monolithic digital to analog converter, to control a DC to DC (low voltage to HV) converter. The buffered output of the HV divider is also multiplexed to a common DVM for computer readout, under control of the digital bus. A similar HV system was built for the Columbia-Stony Brook experiment, for about $50/HV supply, including the crates, bus system and power supplies.

Pulse Height Measurement

An amplifier will be provided for each photomultiplier base. This will allow the photomultiplier anode to terminate in a much higher impedance (1000 Ω rather than 50 Ω) than is usual. Also, the amplifier will provide push-pull output into low cost, high density twisted pair cable, and provide common mode isolation between the detector and the ADC system. Sixteen-channel ADC modules will be provided for the photomultiplier amplifiers, based on an existing design. The twisted pair signal is received differentially and terminated at the ADC. The ADC contains a servo-stabilized linear gate and integrator, and a sixteen-bit Wilkenson type encoder. The integrator charge can be reset in less than 1 μs; this allows the use of a second-level trigger decision, with a 1 μs deadtime, in conjunction with a simpler trigger requiring minimal signal cable delay.

The analog-to-digital encoding involves counting 10 ns bins until the linear ramp equals the integrated charge. Most of the triggers will correspond to calibration with

muons. If we assume minimum ionizing corresponds to channel 100, then 5 x minimum ionizing requires 5 μs of conversion time. The digitized data are scanned at high speed via a bus (common to blocks of 256 ADC channels) into buffer memories during the conversion time. The buffer is split into halves, so that data from the previous event can be transferred to a processor while a new event is loaded into the other half of the buffer. For events involving showers, the maximum possible digitizing time is 160 μs for 16 K bins. To further reduce this time, a mode is provided for automatic range selection, so that for integrator output corresponding to less than 5% of maximum, there are 1024 bins, or 10 μs maximum conversion time; for the remaining 95% of the scale, there are also 1024 bins, or 10 μs maximum conversion time. A programmable charge injector allows calibration of the scale via a precise DC voltage common to the full ADC system.

We estimate the cost of this system, based on an existing 12-bit design, to be about $40/channel, including the photomultiplier amplifier, and readout buffers.

Drift Chamber Readout

We plan to use an existing discriminator and TDC design. The 32-channel discriminators terminate the wires in their characteristic impedance, filter the pulse tails to minimize pulse pileup, and have a minimum threshold of 0.1 μA. The output is standardized in width and amplitude. The discrimination output is push-pull, and drives low cost flat cable.

The TDC receives the signals differentially, to reject common mode noise. Time is measured digitally with respect to the leading edge of a gate. The time span is divided into 64 bins (6 bits), where a bin can be set to any time > 3 μs. Only wire addresses and times corresponding to wire hits are read out. The readout rate can be as high as 50 ns/signal.

The cost/channel is about $20, including the discriminator, the TDC, crates and power supplies.

Interfacing

We will provide the same interface system designed for the Columbia-Stony Brook and Fermilab 605 experiments. This is a very general, high speed data transfer system and includes an interface to the PDP-11 DR-11B data channel. The system also includes buffers that allow recursive trigger processing structures to be added to the readout.

Calorimeter Resolution

Low Z, 100% active calorimetry offers several distinct advantages over the traditional approaches.

1. Energy resolution improves as sampling increases. The energy resolution of the CHARM detector is a factor of ~ two better than resolution attained with 2 in. iron plates.

2. The angular resolution depends to first order on the ratio of the transverse spread of the hadronic shower to the transverse segmentation. In low Z material, this ratio can be made small with reasonable transverse sampling width. This, combined with continuous sampling, allows us to measure energy flow well.

3. Containment of the shower energy in low Z material is difficult. However, since the profile of the shower is measured continuously, the degree of containment can be estimated and corrected for on an event by event basis.

4. Sampling homogeneity is an important difference between the proposed detector and the CHARM calorimeter. Detectors with absorber between scintillation planes will sample showers differently at large angles than small angles, giving rise to possible $P_\perp$ dependent systematics.

The resolution in angle and energy of an all-scintillator calorimeter has never been measured for energies of interest. We estimate the resolution it will attain in two ways.

The closest comparable calorimeter in density is the CHARM marble-scintillator drift-tube detector. Its relevant parameters are $\langle\rho\rangle = 1.3$ g/cm^3, $\langle L_{rad}\rangle = 20$ cm, $\langle L_{abs}\rangle_\pi = 93$ cm; the ratio of sampling to absorber is $\sim 3/8$ and the transverse segmentation is 1.9 rad lengths. The target detector we propose has parameters $\langle\rho\rangle = 1.2$ g/cm^3, $L_{rad} = 34$ cm, $L_{abs\ \pi} = 68.5$ cm, 100% sampling and a transverse segmentation of 0.6 rad lengths. The quoted resolutions for the CHARM calorimeter are

$$\Delta E_h/E_h = 0.01 + 0.43/\sqrt{E_h}$$

and

$$\sigma_\theta = 0.004 + 0.6/E_h \text{ rad}$$

if the vertex of the interaction is known. We will use these resolution as well as the resolution we think we will attain in calculating our sensitivity to a ν_τ signal below.

We have also studied the resolution attainable in our target detector via Monte Carlo simulation of hadronic showers. The showers were generated using a program based on the code developed by A. Grant at CERN (A. Grant, NIM 131, 167 (1975)) and A. Stevens at Brookhaven. The results of this program, using the CHARM calorimeter parameters, agree well with the measured hadron profiles in the CHARM test calorimeter (personal communication, W. Orr) and the quoted CHARM resolutions are reproduced for 20 and 50 GeV π's.

The algorithm we use for finding the direction of the hadron shower first calculates an approximate angle by connecting a straight line between the vertex counter and the counter with maximum pulse height $\sim$ 10 rad lengths into the shower. This establishes a road N counters wide through the shower where N can be varied. A parabola is fitted to each N counter profile and a least squares fit of the parabola centers to a straight line is performed. The new angle can then be used to iterate and check for convergence. Planes whose centers of gravity fall beyond predefined limits from the fitted line can be deleted in the iteration or this information may be used to flag the shower as one whose angle is poorly known. This method is insensitive to the tails of the shower and therefore produces a uniform angular resolution over the entire fiducial volume. If the shower profile indicates that the tail of the shower is not contained in the detector, the event can be flagged and a correction to the hadronic energy made by extrapolating the measured part

of the tail. Thus well measured and well contained showers can be selected on an event-by-event basis.

The results of our study indicate that for this algorithm, the angular resolution in the acrylic scintillator improves by ~ factor of two over the CHARM resolution, while the energy dependence of the resolution remains the same.

The fiducial volume corresponding to a 7.5 mrad acceptance is a 3 ft radius. The transverse size of the target (12 ft x 12 ft) is chosen to maximize containment of the shower while holding the overall tonnage at ~ 200 tons.

Rate Calculations

To calculate rates for prompt neutrino interactions in the detector requires a knowledge of the $D\bar{D}$ production cross section. Results from prompt lepton experiments at 400 GeV vary in the range of 10-40 μb per nucleon, assuming linear A dependence. We assume a central value of 20 μb. Using this number, the prompt ν_μ flux per proton on a copper target can be calculated:

$$\frac{\nu_\mu}{p} = \frac{20\ \mu b}{43\ mb} \cdot \frac{\sigma_{pr}^{1000}}{\sigma_{pr}^{400}} \frac{A^1}{A^{0.72}} Br(D \rightarrow K\mu\nu_\mu) = 0.25 \times 10^{-3} ,$$

where the ratio of cross sections at 400 and 1000 GeV is that predicted by Bourquin-Gaillard. The number of charged current prompt neutrino events in the detector per pulse (2×10^{13} p) can then be calculated as:

$$\text{Events}/2 \times 10^{13}\ p = (\text{Flux})(\text{Target})(\sigma_{cc})\text{Acc}$$
$$= 0.069 \langle E_\nu \rangle \text{Acc} .$$

The only input required from a Monte Carlo is values for the detector acceptance Acc and the average energy of accepted electron neutrinos $\langle E_\nu \rangle$. Both of these numbers depend somewhat on the production mechanism. To illustrate this dependence, we parameterize the invariant cross section for inclusive D production as: $Ed\sigma/d^3p = (1-x)^N e^{-bp}$. We then obtain the number of charged current events expected per pulse (2×10^{13}p) for various values of N and b given in the following table.

b \ N	2	3	4	5	6	7
2	0.75	0.55	0.45	0.35	0.29	0.24
3	0.72	0.54	0.45	0.34	0.28	0.24

These rates are rather insensitive to the value of b. The value of N which is consistent with the energy distribution of prompt neutrino events observed by beam dump experiments is 3. We will use this value in the calculations which follow. The energy spectrum of prompt neutrinos accepted by the detector is shown in Fig. 6.

To calculate a tau neutrino rate, we assume that the primary source of tau neutrinos from a beam dump is the production and decay of the F, $F \rightarrow \tau\nu_\tau$. Per F, there are two tau neutrinos, since the tau also decays:

$$F \rightarrow \tau\nu_\tau$$
$$\quad \hookrightarrow \mu\nu_\mu\nu_\tau$$
$$\quad \hookrightarrow e\nu_e\nu_\tau$$
$$\quad \hookrightarrow h\nu_\tau \qquad (h = \pi,\ \rho,\ A,\ \text{etc.}) \quad .$$

The tau neutrino from F decay has lower energy in the lab than the tau neutrino from the decay of the tau, since the F-τ mass difference is presumed to be small and the τ carries most of the energy of the F. This is clearly seen in the energy distributions in Fig. 6, which show the energy spectrum of tau neutrinos accepted by the detector from the various decay modes. The x and p_t dependence for $F\bar{F}$ production is assumed to be the same as for $D\bar{D}$ production. We also assume that

$$\frac{\sigma \cdot B(F \to \tau \nu_\tau)}{\sigma \cdot B(D \to K \mu \nu_\mu)} = 1/10.$$

In what follows, we consider the contribution to the flux of $\tau \to \nu_\tau X$ only. The angular acceptance of 7.5 mrad corresponds to an $\sim$ 25% acceptance for high energy ν_τ's. The acceptance for ν_μ's from prompt sources is similar. The average energy of interacting ν_τ's is $\sim$ 150 GeV, while the average energy of interacting ν_μ's from $D\bar{D}$'s is $\sim$ 100 GeV.

To demonstrate the existence of the tau neutrino in a neutrino experiment, one must isolate the interaction and decay, $\nu_\tau N \to \tau X$, from the more copious background of ordinary charged current events, $\nu_\mu N \to \mu X$. There are three features of the ν_τ events which are expected to be different. In all three cases, the difference arises from missing energy carried by the two neutrinos in the final state. First, if there is missing energy, there is missing transverse energy. Second, since the observed lepton (μ) carries only

a fraction of the energy of the final state lepton (τ), the x and y distributions will be distorted. Finally, the hadronic shower direction will not be back to back with the muon direction in azimuth, as expected for charged current ν_μ events.

We assume ν_μ events interact via the standard charged current interaction Lagrangian. ν_τ's are assumed to interact via the same Lagrangian (μ-τ universality) but care is taken to keep all the mass terms. We use the following laboratory cross section to model tau production:

$$\frac{d\sigma}{dq^2 d\nu} = \frac{G^2}{8ME^2\pi}\left[2k'\cdot kW_1 + \frac{W_2}{M^2}(k'\cdot kp^2 - 2k'\cdot pk\cdot p) + \frac{2W_3}{M^2}(k'\cdot qk\cdot p - k'\cdot pk\cdot q) + \frac{W_4}{M^2}(k'\cdot kq^2 - 2k'\cdot qk\cdot q) + \frac{W_5}{M^2}(k'\cdot kp\cdot q - k'\cdot pk\cdot q - k'\cdot qk\cdot p)\right],$$

where k' is the tau four vector, k is the incident neutrino four vector and p is the proton four vector. Two new form factors, W_4 and W_5, (suppressed by m_μ/m_p factors in ν_μ interactions) may be important in ν_τ interactions. In what follows, we assume that they are zero. The resulting cross section energy dependence of ν_μ and ν_τ is shown in Fig. 7. The tau is modeled to decay via $\tau \rightarrow \mu\nu\nu_\tau$.

Assuming the flux calculation outlined above and the detector resolutions outlined earlier and an exposure of 2×10^5 pulses of 2×10^{13} protons/pulse, we calculate our sensitivity to a tau neutrino signal.

For events with $E_h > 5$ GeV and $P_\mu > 5$ GeV, we find the acceptance of the muon spectrometer to be $\sim 90\%$ for ν_τ events and essentially 100% for ν_μ C.C. events.

For the assumed 4×10^{18} protons on target, we find 112,000 ν_μ (44,800 $\bar{\nu}_\mu$) and 2500 ν_τ (1000 $\bar{\nu}_\tau$) events. We can form $\vec{P}_\perp^{\,\text{missing}} = \vec{P}_\perp^{\,\mu} - \vec{E}_\perp^{\,\text{hadron}}$ and calculate the x and y variables using the muon four vector and the hadron energy. The distributions in visible energy, missing $P_\perp$, and x and y with experimental resolution folded in, are shown for $\bar{\nu}_\tau$ and $\bar{\nu}_\mu$ in Fig. 8. The visible energy of the two samples is roughly similar, but the P_t missing distribution peaks higher for the ν_τ; the x distribution peaks lower; and the y distribution peaks dramatically higher, having an opposite behavior to the $\bar{\nu}_\mu$ sample. The distributions for ν_τ and ν_μ are similar except for the variable y, where the difference between ν_τ and ν_μ is not as pronounced.

The measurement of $P_\perp^{\text{hadron}}$ and missing transverse momentum is the principal new technique that we propose to use. Since tails on this distribution may be different from the gaussian tails that we have assumed, we first cut on variables which do not depend on the $P_\perp^{\text{hadron}}$ resolution. x and y depend on the muon angle and momentum and the hadron energy. We cut on $x < 0.05$ and $y > 0.5$ to isolate the ν_τ signal. This results in a ratio of $\bar{\nu}_\tau/\bar{\nu}_\mu$ of ~ 0.3. We now plot the projection of the $\vec{P}_\perp^{\,\text{missing}}$ vector onto the $(\vec{\nu}, \vec{\mu})$ plane. Since apart from resolution there is no intrinsic

$P_\perp$ imbalance in ν_μ C.C. interactions (i.e., no missing ν's), the projected $P_\perp^{\text{missing}}$ distribution for these events must be symmetric about $\vec{P}_{\perp\ \text{proj}}^{\ \text{missing}} = 0$.

The $\vec{P}_{\perp\ \text{proj}}^{\ \text{missing}}$ distribution for ν_τ events is skewed to large positive $P_\perp$. The total $\vec{P}_{\perp\ \text{proj}}^{\ \text{missing}}$ distribution after x and y cuts is shown in Fig. 9, assuming CHARM resolutions. Figure 10 shows the same distribution assuming our angular resolution improves over CHARM by a factor of 2. The skew to positive $P_\perp$ implies the existence of a ν_τ signal while the $P_\perp < 0$ distribution indicates the magnitude of the calorimeter $P_\perp$ resolution tail.

Events with a $\overset{(-)}{\nu}_\mu$ in the final state pose a special problem since they will also exhibit missing transverse momentum. The only important source of such events is charmed particle production and its subsequent decay into a semileptonic ($e\nu_e$) final state. We assume all μe events will be confused with normal C.C. events. After $x < 0.05$ and $y > 0.5$ cuts, we estimate $\sim$ 200 ν_μ and 30 $\bar{\nu}_\mu$ such events will remain. These events contribute to the $P_\perp < 0$ side of the $P_{\perp\ \text{proj}}^{\text{missing}}$ plot only. We stress that we will have $\sim$ 1000 identified $\mu^+\mu^-$ events which will allow us to measure the contribution of this background to the $P_{\perp\ \text{proj}}^{\text{missing}}$ distribution.

It should be noted that for $\overset{(-)}{\nu}_\mu$ C.C. events, restricting consideration to $x < 0.05$ and $y > 0.5$ implies that the hadron showers used in the above sample have small forward angles and are high energy, i.e. have minimum problems with energy

Dimuon Final States

$$\bar{\nu} + P \rightarrow \mu^+ + b + \ldots$$
$$\hookrightarrow \mu^- + \ldots$$

One expects that dimuon events associated with charm will dominate over dimuon events associated with bottom by a factor of ~ 100. Hence separating bottom events from charm events is a non-trivial problem which will exercise the unique capabilities of our detector. Because of the larger mass of b states compared to the c states, one will observe a larger $P_\perp$ of the μ^+ normal to the ν_μ-μ^- production plane, as well as a larger $P_\perp^\nu$ carried by the final state neutrinos. Our detector will enable us to compute $P_\perp^\nu$ using the hadron energy flow vector - allowing us to separate charm from bottom through the use of a correlated $P_\perp^\mu$ vs. $P_\perp^\nu$ cut.

Conclusion

The detector considered here offers two unique advantages not available in other neutrino detectors. The muon spectrometer proposed here measures muon bending angles entirely before and entirely after a torroidal bending magnet. It is capable of rapid and efficient reconstruction of complicated multi-muon topologies. We feel that this will be important in completing the construction of the muon shield for beam dump running.

A major emphasis in neutrino physics at the Tevatron will be the study of multimuon final states with missing

neutrinos. We have considered only two of the many possible examples of such states. We are in a unique position to identify and study these states through our accurate measurement of the hadronic energy flow.

Estimate of Costs

Neutrino Target and Hadron Catcher	
Acrylic Scintillator:	$1,213,200
Phototubes, HV and ADC:	460,800
Muon Spectrometer	
Drift Chamber Readout:	70,000
TOTAL	$1,744,000

Figure Captions

Fig. 1 *Bourquin-Gaillard cross sections for $D\bar{D}$, π and K production.*

Fig. 2 Schematic of detector.

Fig. 3 Acrylic scintillator neutrino target assembly.

Fig. 4 Scintillator tube assembly showing sixteen 1/2-in. wide acrylic strips, light pipe, and mechanical support.

Fig. 5 Drift chamber plane construction.

Fig. 6 Energy spectrum of prompt ν_μ and ν_τ neutrinos accepted by detector.

Fig. 7 Energy dependence of ν_μ and ν_τ cross sections.

Fig. 8 Visible energy, actual energy (flux $\cdot \sigma_{CC}$), $|\vec{P}_\perp^{\,\text{missing}}|$, x and y distributions for $\bar{\nu}_\mu$ and $\bar{\nu}_\tau$ events.

Fig. 9 $\vec{P}_\perp^{\,\text{missing}}$ projected on $(\vec{\nu}, \vec{\mu})$ plane for ν_μ and ν_τ events with $x < 0.05$ and $y > 0.5$ assuming CHARM angular and energy resolutions.

Fig. 10 $\vec{P}^{\,\text{missing}}$ projected on $(\vec{\nu}, \vec{\mu})$ plane for ν_μ and ν_τ events with $x < 0.05$ and $y > 0.5$ assuming $\sigma_\theta = \sigma_\theta(\text{CHARM})/2$.

FIGURE 1

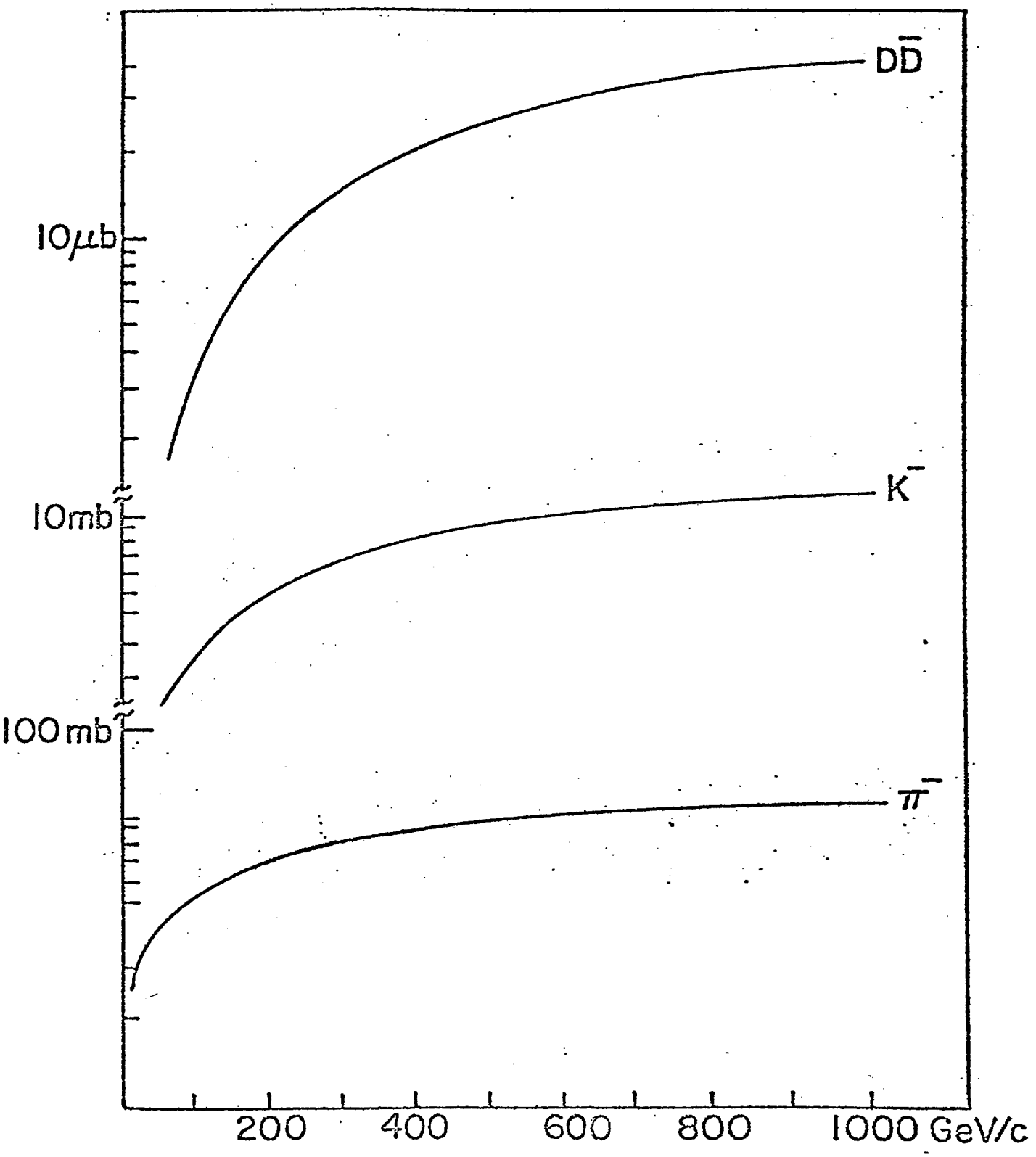

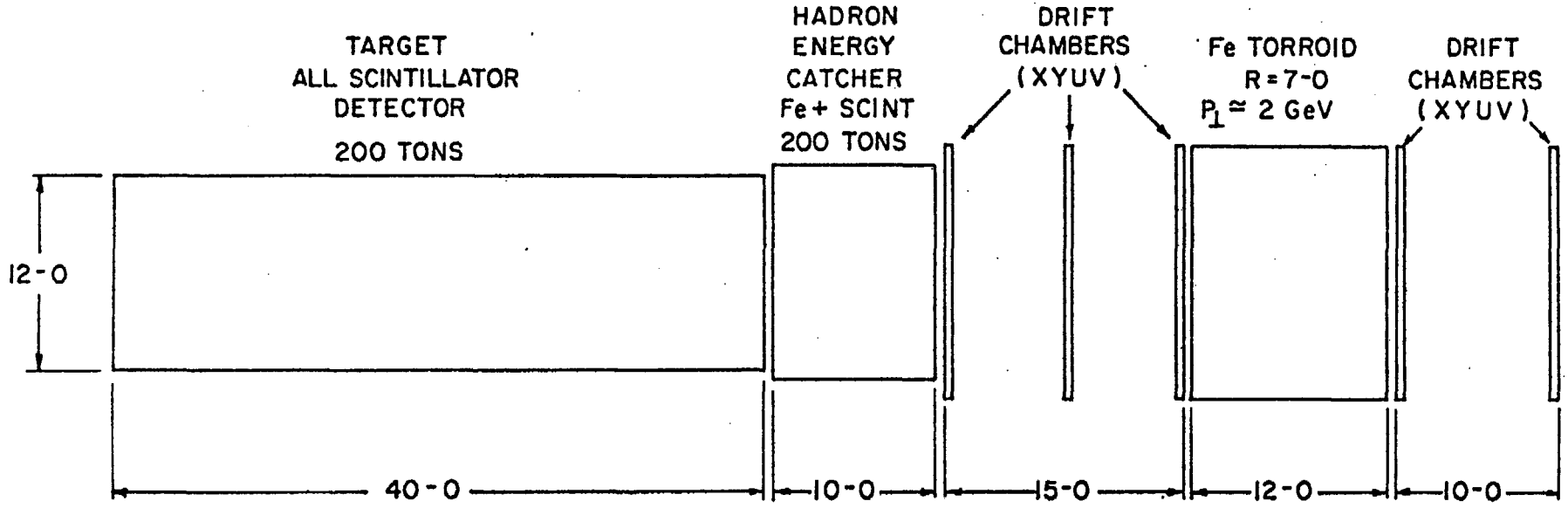
TARGET
ALL SCINTILLATOR
DETECTOR
200 TONS
HADRON
ENERGY
CATCHER
Fe + SCINT
200 TONS
DRIFT
CHAMBERS
(XYUV)
Fe TORROID
R = 7-0
$P_\perp \simeq 2$ GeV
DRIFT
CHAMBERS
(XYUV)
12-0
40-0
10-0
15-0
12-0
10-0

Fig. 2

Fig. 3

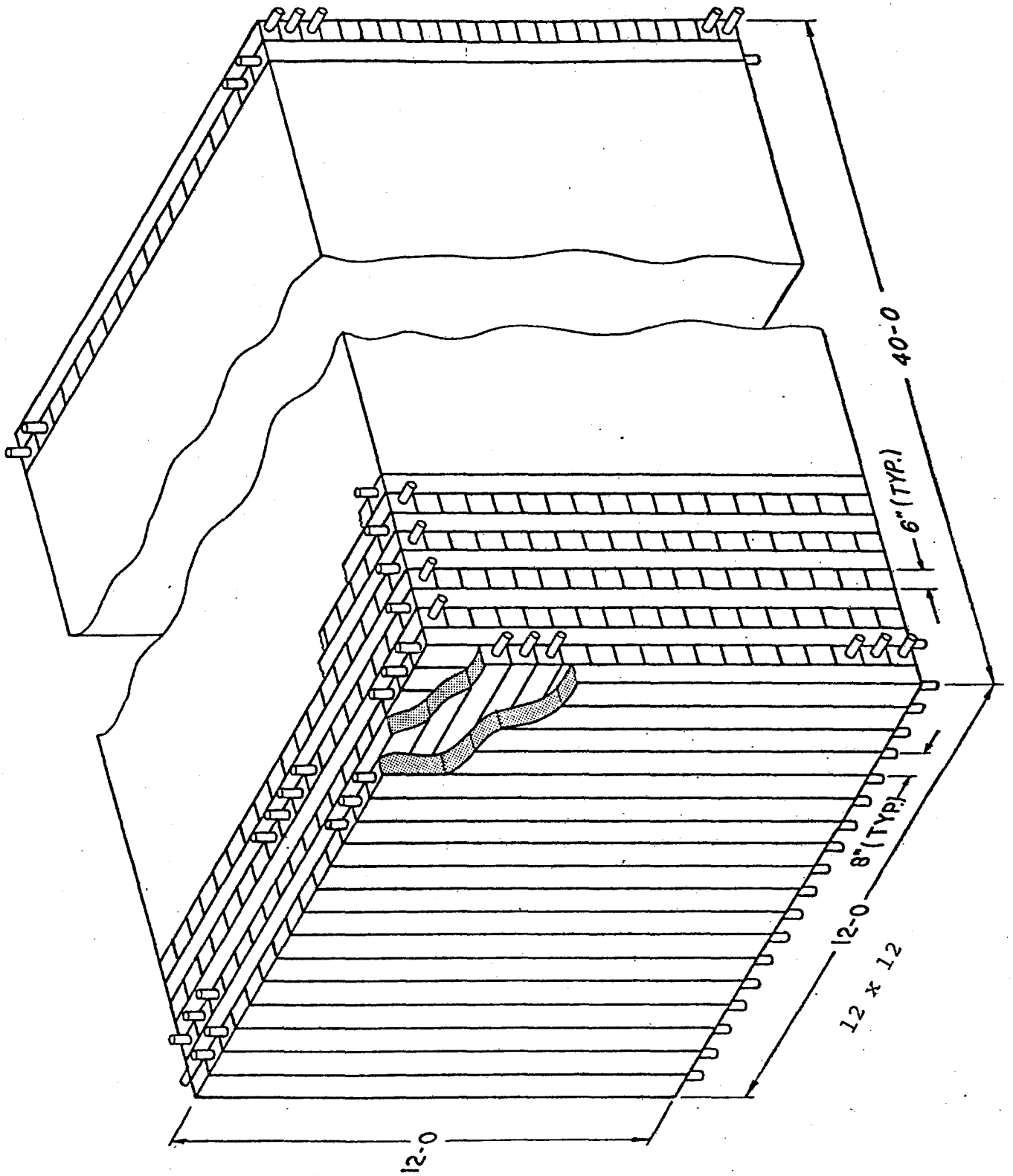

Fig. 4

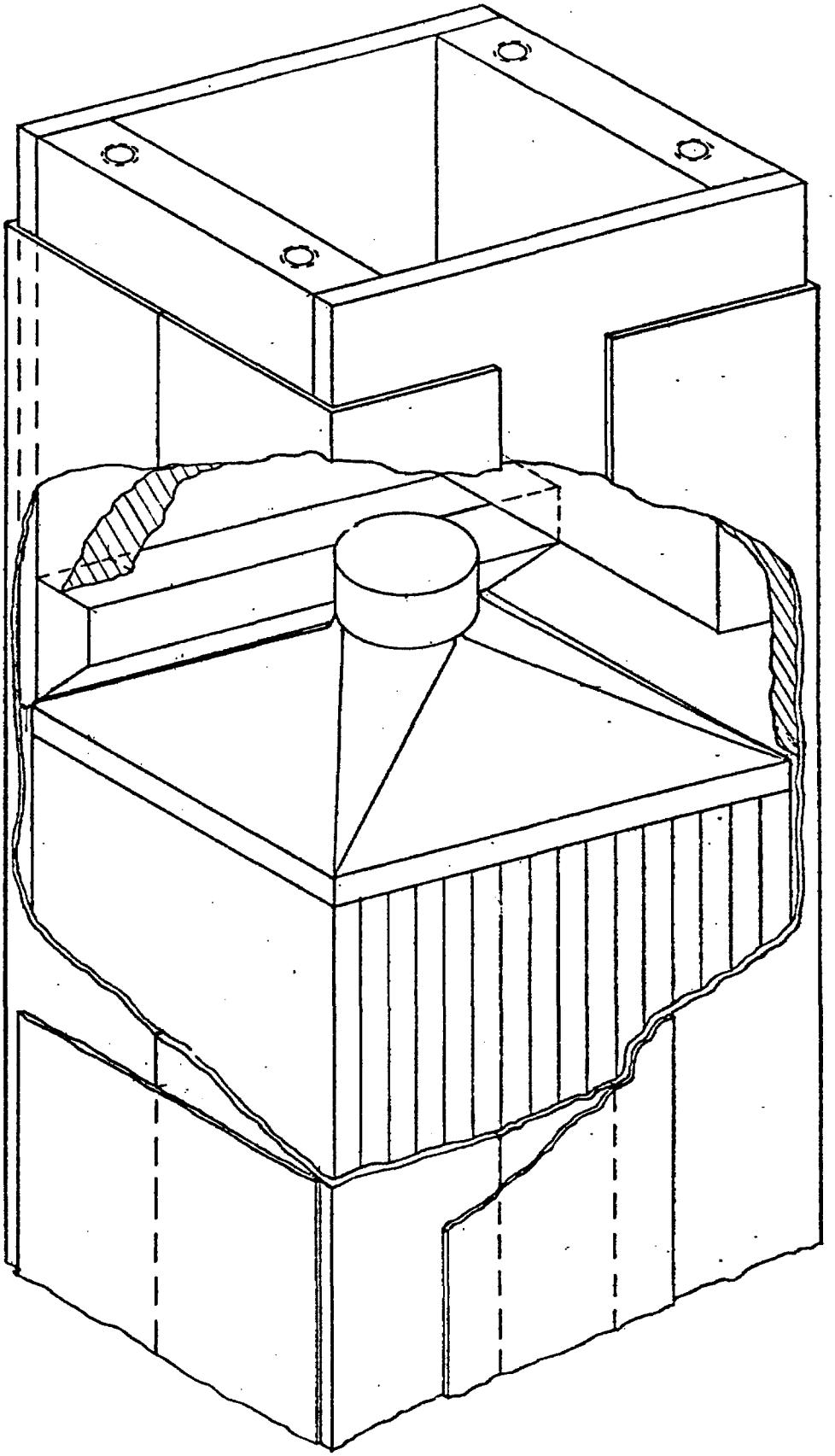

Fig. 5

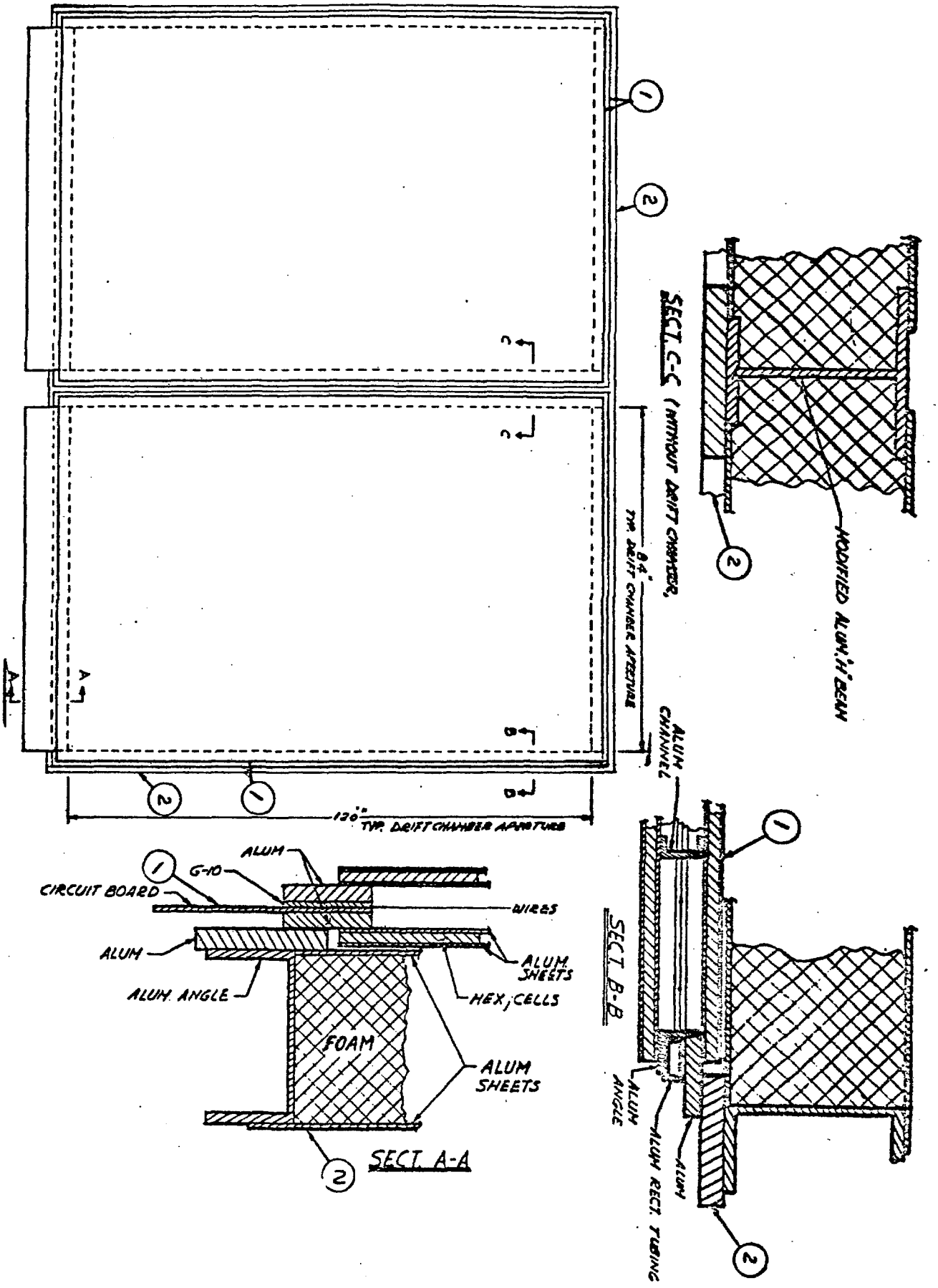
SECT C-C (WITHOUT DRIFT CHAMBER)
MODIFIED ALUM. I BEAM
ALUM CHANNEL
SECT B-B
ALUM ANGLE
ALUM RECT. TUBING
ALUM
CIRCUIT BOARD
G-10
WIRES
ALUM
ALUM. SHEETS
ALUM. ANGLE
HEX. CELLS
FOAM
ALUM SHEETS
SECT A-A
TYP. DRIFT CHAMBER APERTURE

Fig. 6

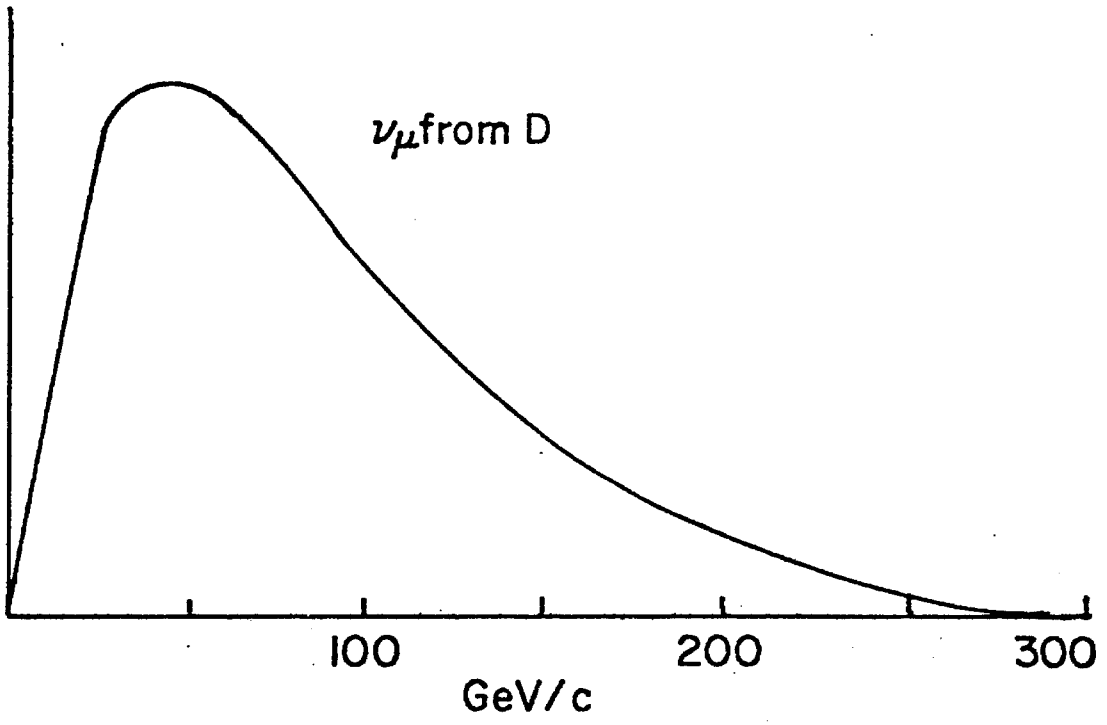
ν_μ from D
100
200
300
GeV/c

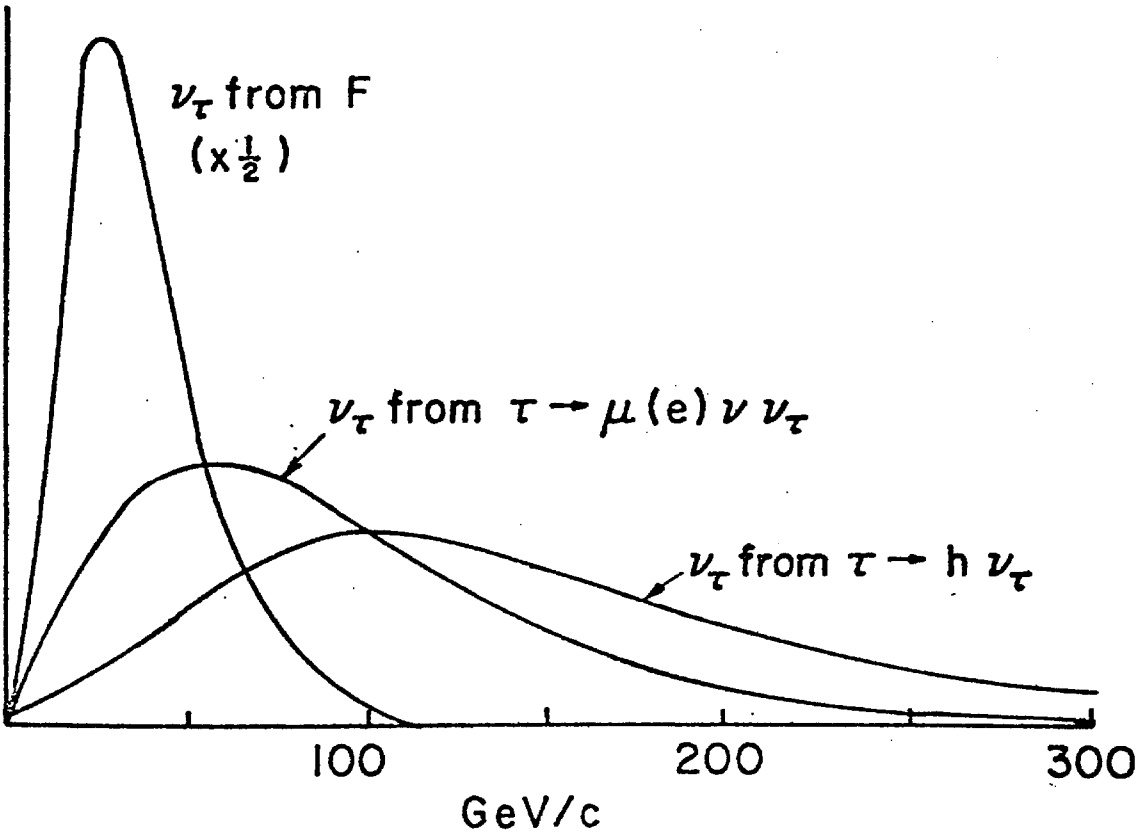
ν_τ from F
($\times\frac{1}{2}$)
ν_τ from $\tau \to \mu$ (e) $\nu\ \nu_\tau$
ν_τ from $\tau \to$ h ν_τ
100
200
300
GeV/c

Fig. 7

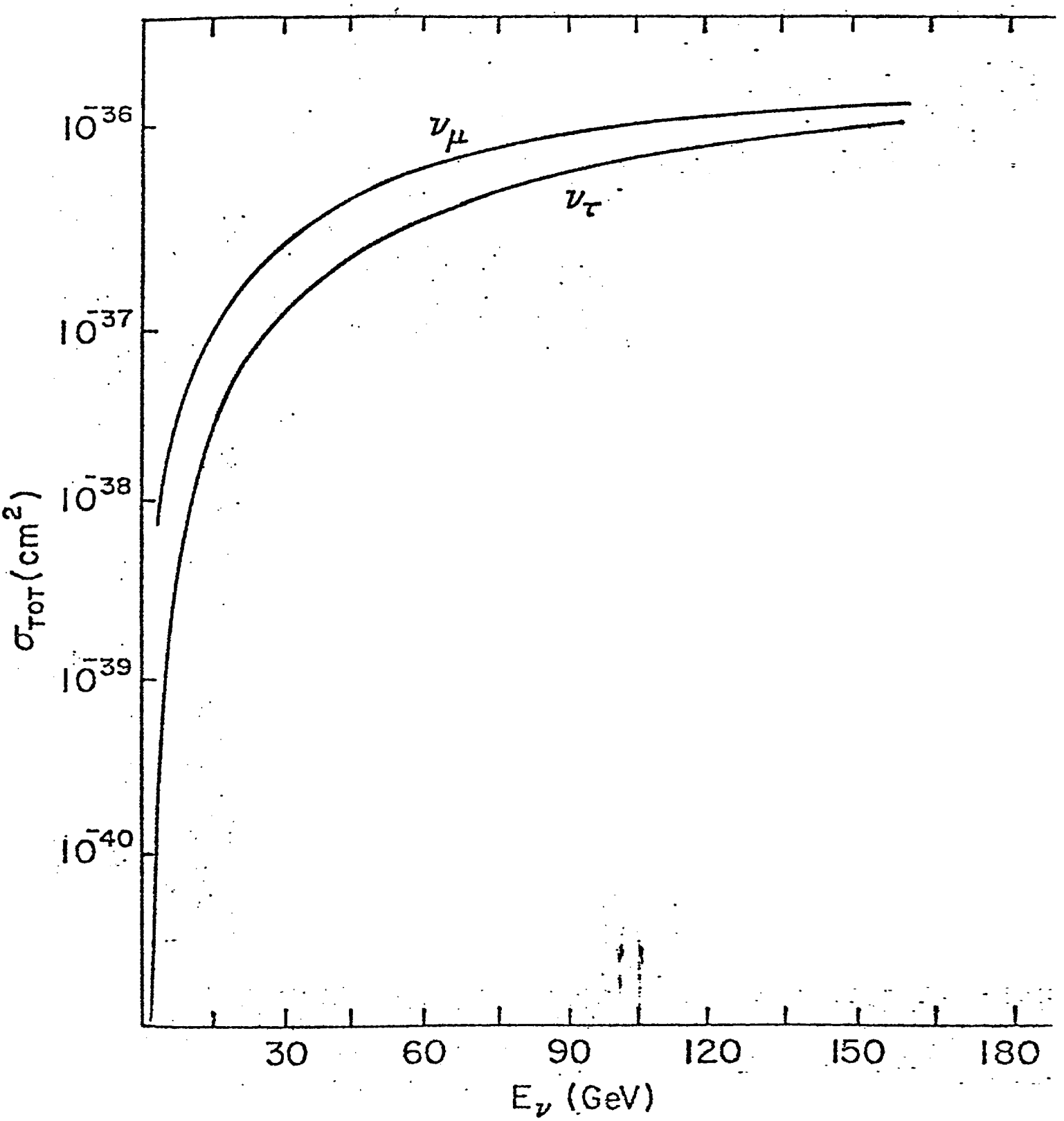
10^{-36}
10^{-37}
10^{-38}
10^{-39}
10^{-40}
$\sigma_{TOT}(cm^2)$
ν_μ
ν_τ
30
60
90
120
150
180
E_ν (GeV)

Fig. 8

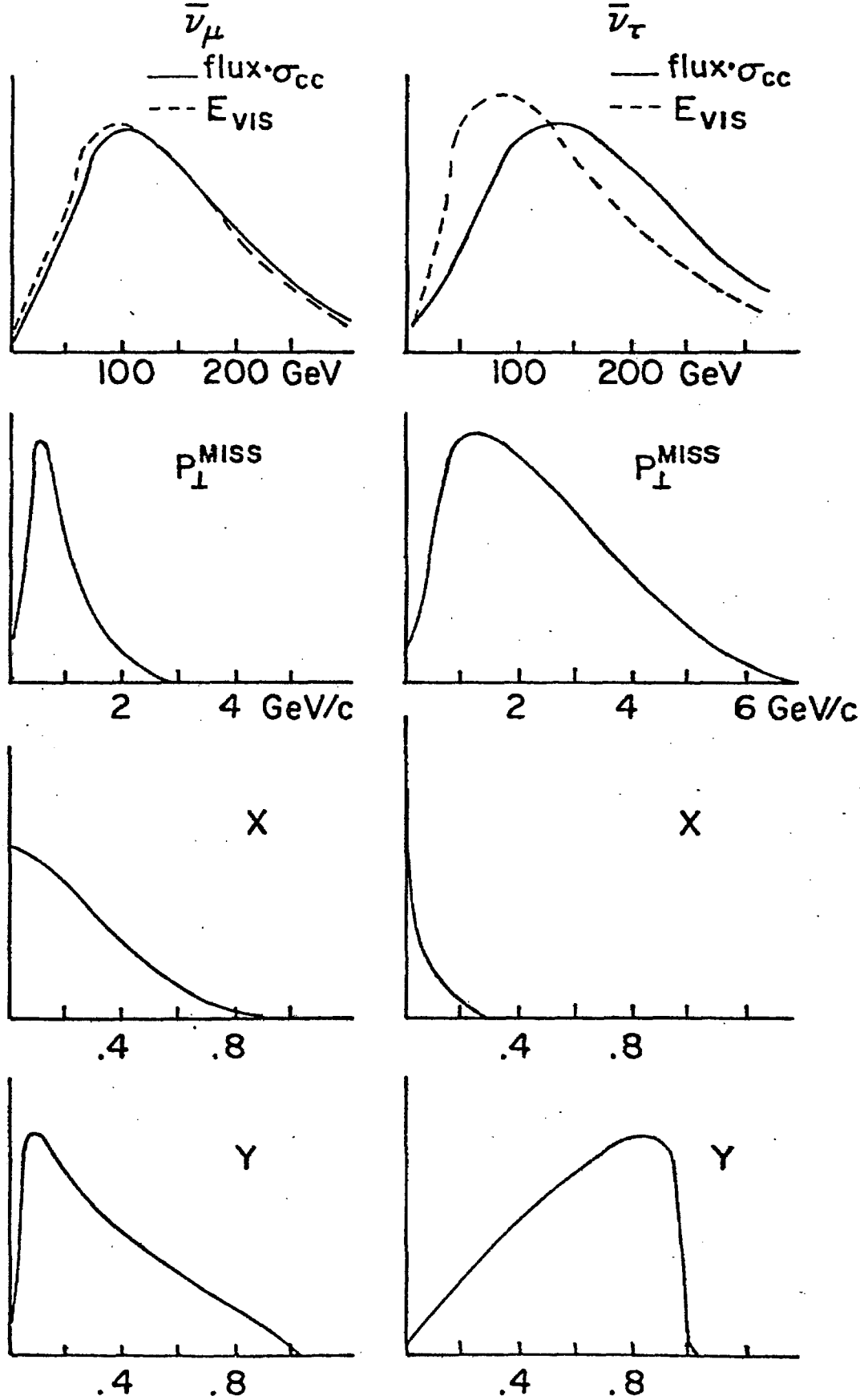
$\bar{\nu}_\mu$
flux·σ_{cc}
E_{VIS}
100
200 GeV
$\bar{\nu}_\tau$
flux·σ_{cc}
E_{VIS}
100
200 GeV
$P_\perp^{MISS}$
2
4 GeV/c
$P_\perp^{MISS}$
2
4
6 GeV/c
X
.4
.8
X
.4
.8
Y
.4
.8
Y
.4
.8

Fig. 9

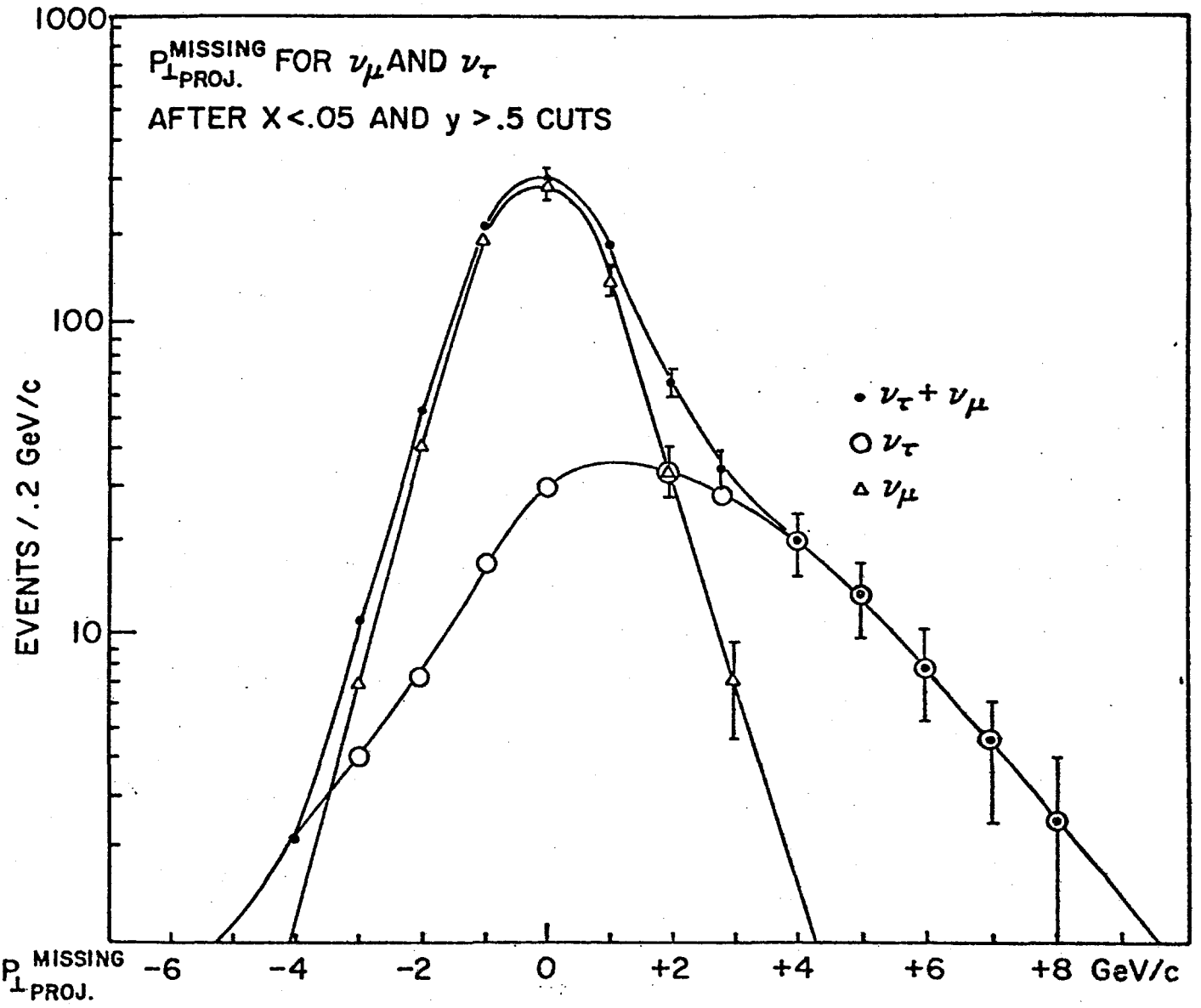
1000
100
10
EVENTS / .2 GeV/c
$P_{\perp PROJ.}^{MISSING}$ FOR ν_μ AND ν_τ
AFTER X<.05 AND y >.5 CUTS
• $\nu_\tau + \nu_\mu$
○ ν_τ
△ ν_μ
$P_{\perp PROJ.}^{MISSING}$
-6
-4
-2
0
+2
+4
+6
+8 GeV/c

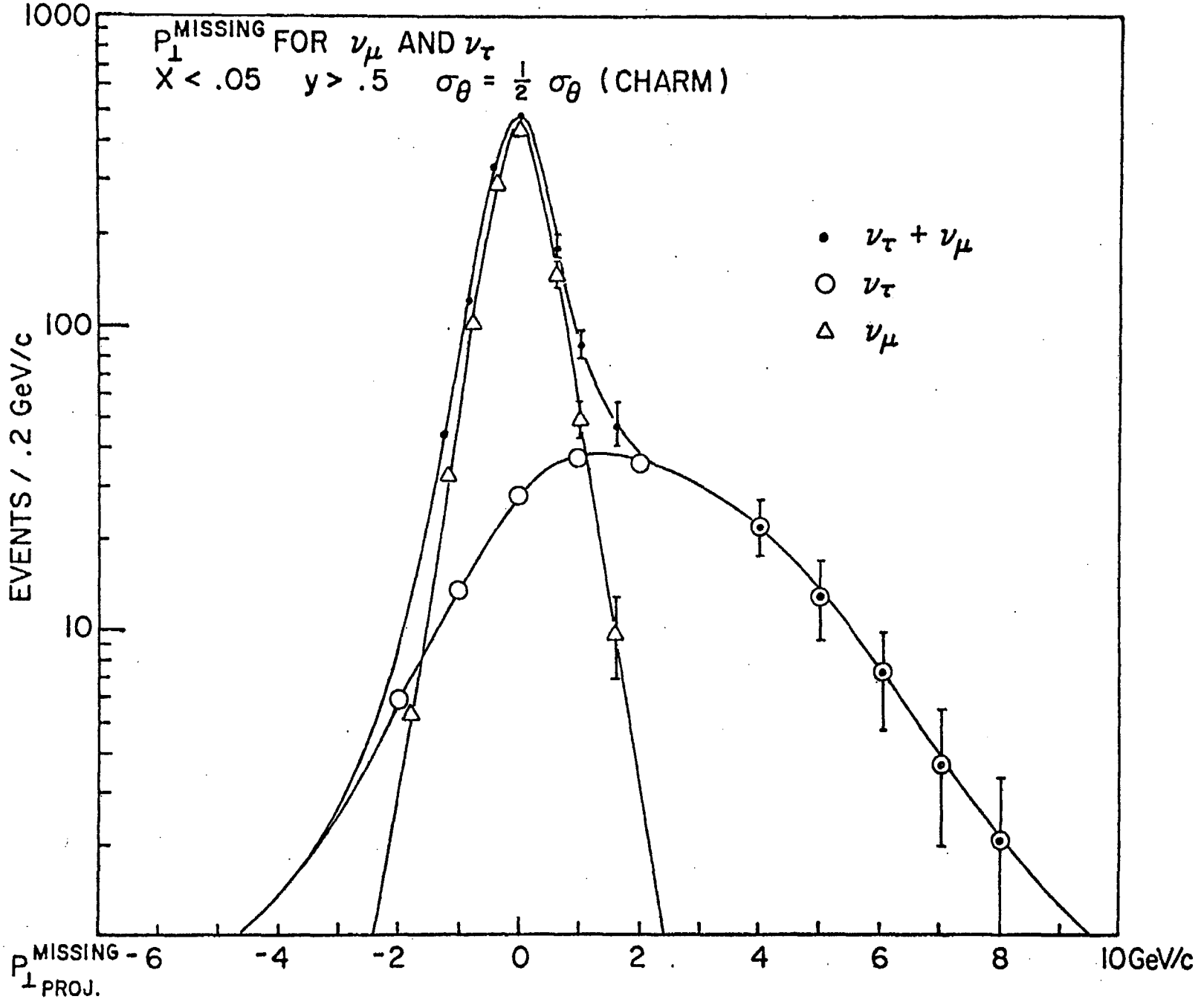
1000
100
10
EVENTS / .2 GeV/c
$P_\perp^{MISSING}$ FOR ν_μ AND ν_τ
X < .05 y > .5 $\sigma_\theta = \frac{1}{2}\sigma_\theta$ (CHARM)
• $\nu_\tau + \nu_\mu$
○ ν_τ
△ ν_μ
-6
-4
-2
0
2
4
6
8
10GeV/c
$P_{\perp PROJ.}^{MISSING}$

Fig. 10